JCB Article

Filopodia and actin arcs guide the assembly and transport of two populations of microtubules with unique dynamic parameters in neuronal growth cones

Andrew W. Schaefer, Nurul Kabir, and Paul Forscher

Yale University, New Haven, CT 06520

We have used multimode fluorescent speckle microscopy (FSM) and correlative differential interference contrast imaging to investigate the actin–microtubule (MT) interactions and polymer dynamics known to play a fundamental role in growth cone guidance. We report that MTs explore the peripheral domain (P-domain), exhibiting classical properties of dynamic instability. MT extension occurs preferentially along filopodia, which function as MT polymerization guides. Filopodial bundles undergo retrograde flow and also transport MTs. Thus, distal MT position is determined by the rate of plus-end MT assembly minus the rate of retrograde F-actin flow. Short MT displacements independent of flow are sometimes observed. MTs loop, buckle, and break as they are transported into the T-zone by retrograde flow. MT breakage results in exposure of new plus ends which can regrow, and minus ends which rapidly undergo catastrophes, resulting in efficient MT turnover. We also report a previously undetected presence of F-actin arc structures, which exhibit persistent retrograde movement across the T-zone into the central domain (C-domain) at ~1/4 the rate of P-domain flow. Actin arcs interact with MTs and transport them into the C-domain. Interestingly, although the MTs associated with arcs are less dynamic than P-domain MTs, they elongate efficiently as a result of markedly lower catastrophe frequencies.

Introduction

In the neuronal growth cone, a sharp, yet highly dynamic interface exists between growing microtubles (MTs)* in the axon shaft, and peripheral actin networks. Mounting evidence suggests that directed axon guidance depends on coordinated interactions between MTs and actin filaments in growth cones (Suter and Forscher, 2000). During axon guidance, actin based motility is harnessed to promote MT growth and steering. However, the fundamental details of how F-actin networks influence MT behavior, and visa versa, are not well understood. MT behavior in growth cones was initially characterized by Tanaka and Kirschner (1995) (also Sabry et al., 1991). They found that individual unbundled MTs invaded the actin-rich peripheral domain (P-domain) and appeared to display properties of dynamic instability; however, because it was not possible to make fiducial marks on MTs, the respective contributions of polymerization and translocation to MT advance could not be assessed. Damping MT dynamics with vinblastine (without net depolymerization) disrupted the normal cycle of MT bundling and splaying, but actin-based motility was essentially unimpaired. Interestingly, vinblastine-treated growth cones tended to wander, suggesting that MT dynamics are necessary for converting actin-based motility into directed, persistent growth (Tanaka et al., 1995). Subsequent reports confirmed that dampening MT dynamics also inhibited growth cone turning in response to guidance cues (Tanaka and Kirschner, 1995; Williamson et al., 1996; Challacombe et al., 1997).

Hints that actin motility is an early step in axon guidance responses emerged from studies where F-actin accumulated in growth cone filopodia before turning (O'Connor and Bentley, 1993). In particular, there has been much speculation about the function of filopodia. Evidence suggests that filopodia can play a structural role, exert mechanical tension, selectively adhere to target substrates, and are involved in signal transduction (Davenport et al., 1993; Gomez et al., 2001). EM and immunofluorescence studies have also noted striking coalignment of filopodial F-actin bundles with MTs in growth cones (Letourneau, 1983; Gordon-Weeks, 1991;

The online version of this article contains supplemental material.

Address correspondence to Paul Forscher, Department of Molecular, Cellular, and Developmental Biology, KBT222, Yale University, P.O. Box 208103, New Haven, CT 06520-8103. Tel.: (203) 432-6344. Fax: (203) 432-8999. E-mail: paul.forscher@yale.edu

*Abbreviations used in this paper: C-domain, central-domain; DIC, differential interference contrast; FSM, fluorescent speckle microscopy; MT, microtubule; P-domain, peripheral domain; ROI, region of interest; T-zone, transition zone.

Key words: microtubules; axon outgrowth; actin; growth cone; dynamics

Bush et al., 1996). These observations led to the notion that capture or stabilization of dynamic MT ends via interactions with filopodial actin bundles may be an early step in growth cone turning (Gordon-Weeks, 1991; Sabry et al., 1991; Challacombe et al., 1996, 1997; Williamson et al., 1996). It is also well known that growth cones use actomyosin- based motility to exert steering forces on substrates (Bray, 1979; Lamoureux et al., 1989). Not surprisingly, cytochalasin treatments resulted in loss of axon and MT guidance capabilities (Bentley and Toroian-Raymond, 1986), although axonal MTs can still extend randomly in the absence of actin assembly (Marsh and Letourneau, 1984). MTs were also observed to rapidly extend to the leading edge of growth cones treated with cytochalasin after clearance of P-domain F-actin (Forscher and Smith, 1988), again suggesting intimate MT–actin interactions. In complimentary experiments, damping MT dynamics (with taxol or low doses of MT assembly inhibitors) did not markedly affect retrograde F-actin flow; however, MTs were cleared from the P-domain (Rochlin et al., 1996; Williamson et al., 1996; Challacombe et al., 1997; Kabir et al., 2001), suggesting retrograde actin flow may regulate MT positioning. Indeed, recent studies in motile cells have demonstrated that retrograde F-actin flow affects MT translocation, assembly, and catastrophe rates (Waterman-Storer and Salmon, 1997). All of these observations point to the importance of MT–actin filament interactions; however, a clear description of how these two cytoskeletal polymers influence each other's behavior in growth cones has not emerged.

Recent advances in cooled CCD-based imaging techniques, including multimode fluorescent speckle microscopy (FSM), make it possible to directly measure actin and tubulin polymer dynamics in living cells, and correlate them with cell motility (Waterman-Storer and Salmon, 1998; Waterman-Storer et al., 1998). In the current study we have used FSM to determine the relative contribution of MT assembly dynamics versus MT translocation in establishing the steady-state MT distribution in growth cones, and to address how F-actin dynamics influence MT behavior. This data provides a quantitative framework for interpreting the complex effects of signaling pathways on the cytoskeletal motility machinery during axon growth and guidance (Song and Poo, 1999). We focus on three findings: (1) filopodia are assembly guides for a highly dynamic population of MTs that efficiently explore the P-domain; (2) actin filament arc structures in the T-zone are associated with a population of MTs with distinctly different kinetic parameters than those in the P-domain; and (3) filopodia and arcs both transport MTs.

Results

MT–actin filament interactions: a structural perspective

The FSM studies in this report provide new insights into MT–actin filament dynamics in living growth cones; they also prompted us to look more closely at the cytoskeletal structures involved. To this end, we have adapted protocols for high resolution immunocytochemical and ultrastructural analysis of the cytoskeleton in *Aplysia* growth cones after Svitkina et al. (1995). Fig. 1 (A–C) shows a growth cone extracted with TX-100 in a cytoskeletal stabilizing buffer, and then fixed and labeled for actin filaments (Fig. 1 A) and β-tubulin (Fig. 1 B). The P-domains and the central domains (C-domains), separated by the transition zone (T-zone), are indicated (Fig. 1 A; Forscher and Smith, 1988; Lin et al., 1994). Two F-actin structures are germane to the current report: (1) filopodia, composed of unipolar actin filament bundles, that span the width of P-domain and often extend distally past the leading edge (Lewis and Bridgman, 1992); and (2) arc-shaped F-actin bundles (Fig. 1 A, arrowheads) located in the T-zone. The latter structures resemble the retrograde moving actin arcs originally described by Heath (1983) in motile fibroblasts, and we will maintain this nomenclature here. MTs extending into the P-domain are often closely associated with filopodial F-actin bundles (Fig. 1 C, arrowhead), both in fixed cells and in live cell imaging studies (Kabir et al., 2001). Interestingly, arcs are also closely associated with MTs. This is especially evident in lateral T-zone domains orthogonal to the axis of growth cone advance (Fig. 1 C, arrow). Fig. 1 (D–F) shows the growth cone cytoskeletal ultrastructure visualized with tungsten replica rotary shadowing transmission EM. F-actin bundles comprising filopodia are prominent features of the P-domain (Fig. 1, D, red box, and F, higher magnification). Filopodia appear to be intercalated in a less organized actin filament meshwork. Note the high density of short filaments, many with exposed ends (Fig. 1 F, green arrows), residing in an ~3-μm wide band at the leading edge, where barbed-end filament assembly is coordinated to support retrograde F-actin flow (Forscher and Smith, 1988). The ultrastructural features described here appear similar to those in vertebrate growth cones (Lewis and Bridgman, 1992). The striking degree of physical contiguity between the P- and C-domains is notable given that massive actin filament recycling must occur in the T-zone to maintain retrograde F-actin flow. These images suggest this occurs by a mechanism that does not compromise the structural integrity of the C- to P-domain connection. In the C-domain, intertwined filamentous structures with distinct diameters are clearly present (Fig. 1 E). β-Tubulin immunogold labeling was performed to identify MTs. A high magnification of the T-zone–P-domain interface (analogous to Fig. 1 F, arrowhead) is shown in Fig. 1 G. Gold particles (white dots) label four MTs in this field, one of which (MT tip, blue arrow) is caught just entering the proximal base of a filopodial actin bundle (green arrowhead). Note the close apposition of the distal MT segment with the actin bundle. MT loops (Fig. 1 B, arrowhead) where MTs were not in close contact with actin bundles were also observed. Fig. 1 H is a representative sample of the P-domain, showing three MTs tracking along branching F-actin bundle structures (gold-labeled MTs pseudocolored red for clarity). A more detailed immuno-EM characterization of the bag cell growth cone cytoskeleton ultrastructure will be reported separately.

Two distinct zones of retrograde F-actin flow

Retrograde F-actin flow has been well characterized in *Aplysia* bag cell neuron growth cones by fluorescence photobleaching of actin and phalloidin probes (Lin and Forscher, 1995) and analysis of flow coupled extracellular bead movements (Lin and Forscher, 1993; Lin et al., 1996). In the present FSM studies we extend these findings, using low

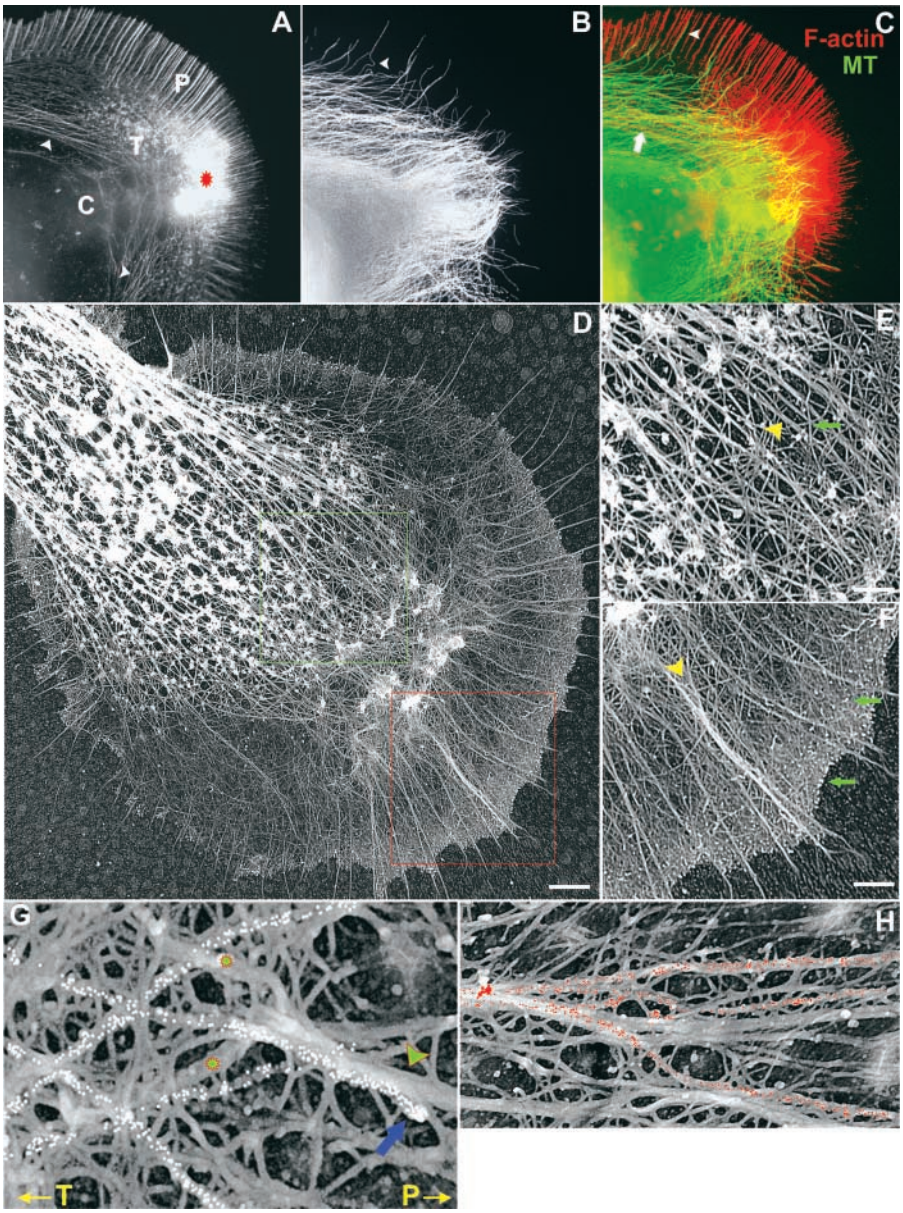

Figure 1. **Structural organization of the growth cone reveals codistribution of MTs with two distinct zones of F-actin structure.** (A) F-actin; C, C-domain; P, P-domain; T, transition zone; arrowheads indicate arcs, most evident on lateral aspects of growth cone; red star marks a ruffling focus. (B) MTs; Arrowhead indicates loop. (C) F-actin/MT overlay; arrow indicates arc-MT colocalization; arrowhead indicates MT-filopodium coalignment. (D) Low magnification rotary shadow electron micrograph of bag cell growth cone cytoskeleton. Bar, 3.5 μm. (E) Higher magnification of C-domains (D, green box); arrowhead denotes MT; green arrow denotes actin filament. (F) Higher magnification of P-domain (D, red box); green arrows denote actin filament ends; arrowhead splayed filopodium. Bars (E–F): 1.75 μm. (G) MT–actin filament interactions in T-zone–P-domain interface. Gold particles (white dots) label four MTs; blue arrow indicates MT entering the proximal base of a filopodial actin bundle (green arrowhead). (H) Lower magnification of P-domain showing three MTs tracking along branching F-actin bundle structures. Immuno-gold MT label is pseudocolored red for clarity. (G–H) Gold particles, 15 nm.

concentrations of injected alexa-phalloidin to generate fiducial marks (speckles) on actin filament structures to study their dynamic properties. Fluorescently labeled phalloidin was chosen as a probe because it preferentially binds filaments, yielding higher signal/noise levels than G-actin probes for assessing F-actin movements. Note that the cellular phalloidin concentrations used for FSM were ~1/5 of that used previously to characterize F-actin flow in this system, and well below levels that perturb F-actin flow (Lin and Forscher, 1995; see Materials and methods). Fig. 2 A (Video 1, available at http://www.jcb.org/cgi/content/full/jcb.200203038/DC1) shows the pattern of F-actin labeling in a living growth cone after image processing to enhance speckle contrast. In the P-domain, both radial filopodia arrays and intervening networks are labeled; however, filopodia are most prominent, likely due to the high density of relatively stable actin filaments they contain. Note that the intensity of F-actin labeling is low in the distal P-domain and increases near the T-zone boundary. This is likely due to the slow association rate constant for phalloidin (De La Cruz and Pollard, 1996) and not actual actin filament density. The latter can be appreciated in fixed cells (Fig 1 A), which have a high density of phalloidin-positive actin filaments throughout the P-domain (Fig. 1 F) or cells injected with labeled G-actin (unpublished data). An example of a growth cone injected with a higher concentration (~5 μM cellular) of phalloidin is included in the online supplemental materials for comparison (Video 3, available at http://www.jcb.org/cgi/content/full/jcb.200203038/DC1; note absence of obvious speckle patterns, labeling of regions between filopodial bundles, and that retrograde flow is unperturbed even at this [~2.5-fold]-higher phalloidin level).

Typically, the C-domain has punctate F-actin labeling. This F-actin pattern is not observed in TX-100–extracted fixed preparations, suggesting a membrane association (e.g. Fig. 1). Complex F-actin movements are observed here that deserve further characterization (Fig. 2, B and C). Speckles within filopodia can readily be followed over time as they

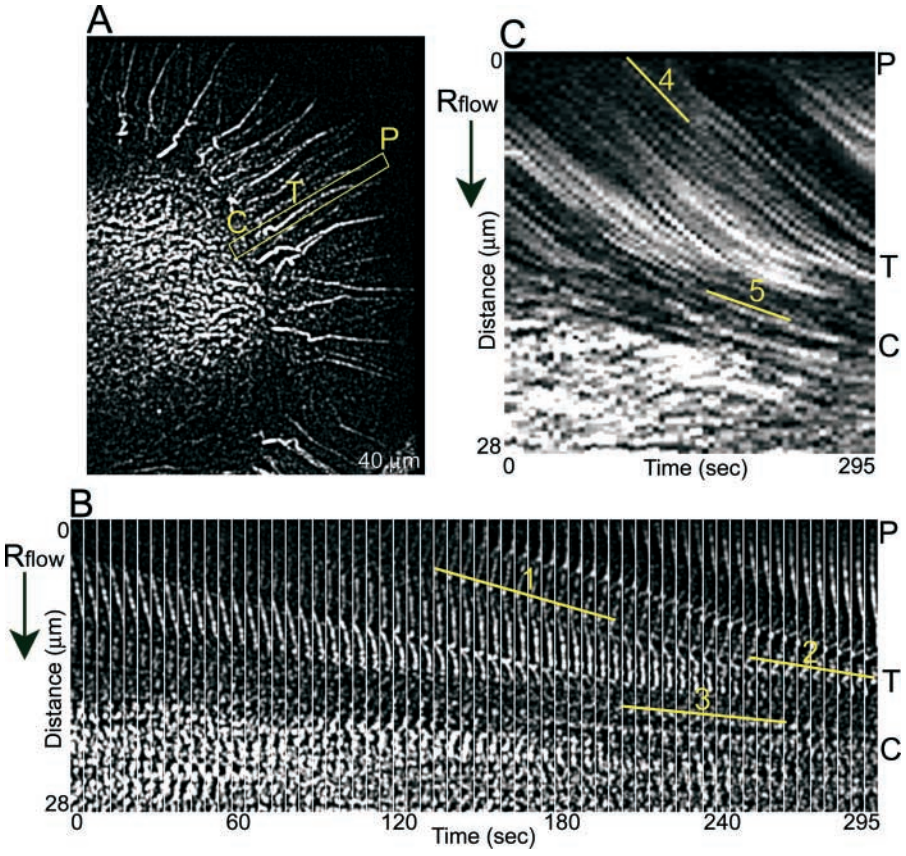

Figure 2. **The growth cone has two zones of retrograde F-actin flow.** (A) Global view of retrograde flow in a growth cone visualized with FSM. Neuron injected with alexa-594 phalloidin. (B) Time-lapse montage of ROI (box in A from P- to C-domain). Note the peripheral actin cables bend and kink as they slow and enter the transition zone. A speckle is followed with yellow lines as it moves toward the transition zone and slows from 4.9 μm min^{-1} (line 1) to 3 μm min^{-1} (line 2). Second zone of slower flow emerges proximal to the transition zone (line 3). (C) Kymograph of ROI. Slopes of speckles are parallel in P-domain and converge at T-zone as the flow slows. Fast flow zone line 4 (5.2 μm min^{-1}); slow flow zone line 5 (1.3 μm min^{-1}). C, central domain; P, peripheral domain; T, transition zone.

move though the P-domain and into the T-zone (Fig. 2 B [Video 2, available at http://www.jcb.org/cgi/content/full/jcb.200203038/DC1]) where filopodia appear to be severed and disassemble by an uncharacterized mechanism. Rates of retrograde flow assessed directly from speckle displacements over time do not differ significantly from previously published values assessed with fluorescence photobleaching or flow coupled beads (Lin and Forscher, 1995; Fig. 2 C, line 1 slope = 4.9 μm min^{-1}). As individual speckles moved into the T-zone, they kink as previously described (Fig. 2 A; Forscher and Smith, 1988) and their translocation rate slows abruptly (Fig. 2 B, compare lines 1 and 2), consistent with previous observations using flow-coupled beads (Forscher and Smith, 1990). Fig. 2 C is a kymograph (space versus time plot) obtained from the regions of interest (ROI) in Fig. 2 A. Retrograde movement of individual speckles over time creates a series of diagonal stripes in the kymograph, their slope indicating the velocity of F-actin movement. The presence of many parallel speckle lines in the P-domain (top 1/2 of kymograph) demonstrates the uniform rate of retrograde flow over time (Lin et al., 1996) and strongly suggests that actin networks are not undergoing contraction or compression here. In contrast, as speckles approach the T-zone, there is clear evidence of network compression and/or contraction, indicated by the convergence of speckle tracks. The fact that filopodia kink as their translocation rate slows in the T-zone, also suggests filopodia are not being pulled in by a force applied to their proximal ends.

These experiments also revealed previously undetected retrograde F-actin movements in the T-zone proceeding toward the C-domain boundary at ~1/4 the rate of P-domain flow (Fig. 2 B, line 3 [Video 2, available at http://www.jcb.org/cgi/content/full/jcb.200203038/DC1]). This slower retrograde flow is apparent in both the kymograph and time montage (compare lines 5 and 3, respectively) and is due to movement of the actin arcs described above. Arcs appear to form in the T-zone and are more easily visualized on the lateral aspects of growth cones (Fig. 1) and will be

Table I. **Microtubule dynamic parameters**

Parameter	Plus-end periphery	Plus-end actin arc associated	Minus-end periphery
Growth	6.9 ± 0.3	3.82 ± 1.4	–
Shortening	−11.5 ± 0.5	−3.06 ± 1.3	−5.62 ± 2.6
Catastrophe frequency	1.00	0.281	–
Rescue frequency	1.40	5.68	–
Percentage of time in growth	41.6	45.5	0
Percentage of time in shortening	25.0	5.0	59
Percentage of time in pause	33.4	49.5	41

Plus-end periphery (n = 49 MTs), plus-end shortening (n = 31 MTs) , and minus-end shortening (16 MTs); rates are μm min^{-1} ± sem. Catastrophe and rescue frequencies are min^{-1}. Data compiled from 12 growth cones. Fluorescence images were collected a 5-, 10-, or 12-s intervals for 240–500 s of elapsed time.

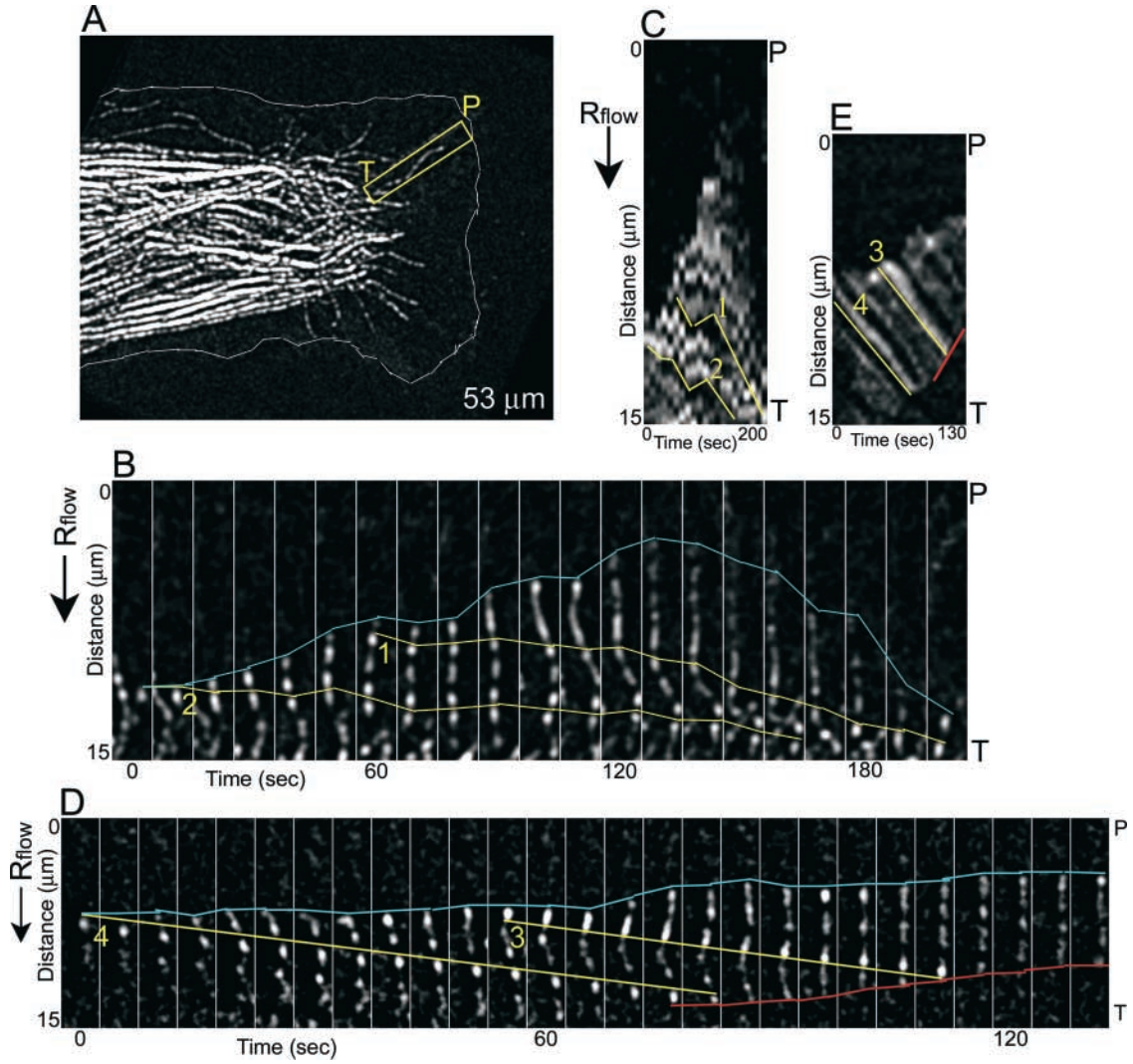

Figure 3. **Single MTs enter the periphery by polymerization and are cleared by catastrophes and retrograde translocation.** (A) Global view of MT dynamics visualized with FSM. Neuron injected with rhodamine-conjugated tubulin. (B) Time-lapse montage of ROI in A. Typical behavior of P-domain MTs. A single MT polymerizes into periphery, undergoes retrograde translocation, and experiences catastrophe. Note retrograde translocation rate tends to increase as MT extends further into periphery; compare the slopes of lines 1 and 2. (C) Kymograph of B. (D and E) Time-lapse montage and kymograph of another MT that grows into periphery at an average rate of 7.4 μm min^{-1}, nearly the same rate at which it translocates rearward toward T-zone (lines 3 and 4). Thus, its apparent growth rate is only ~1.6 μm min^{-1}. Blue line marks distal MT speckle, and yellow lines mark internal reference speckles. Red line marks minus end coming into view which shortens at 7.6 μm min^{-1}.

considered further below in the context of their novel MT organizing capacity. In summary, retrograde flow and arc translocation rates were 4.5 ± 0.5 and 1.0 ± 0.3 μm/min, respectively (rates ± SEM compiled from six growth cones, five measurements per growth cone. Fluorescence images were collected at 5- or 10-s intervals for 240–500 s of elapsed time).

Effects of MT dynamics on MT position

Under control conditions, single MTs tend to enter the P-domain by growth (polymerization) and are cleared from the periphery by a combination of catastrophe events and retrograde translocation (Kabir et al., 2001). Fig. 3 A (Video 4, available at http://www.jcb.org/cgi/content/full/jcb.200203038/DC1) shows a typical distribution of MTs in a live neuron injected with rhodamine-tubulin at a level appropriate for FSM. The time-lapse montage in Fig. 3 B (Video 5, available at http://www.jcb.org/cgi/content/full/jcb.200203038/DC1) shows the behavior of the MT indicated in the ROI (Fig. 3 A), over a 200-s interval. This MT undergoes ~120 s of sustained growth (increasing distance between internal reference speckles [yellow lines] and distal end speckle [blue line]), pauses for 30 s, and then experiences a catastrophe while undergoing simultaneous retrograde translocation. The pattern of growth and retrograde MT displacement can also be seen in the kymograph (Fig. 3 C). Fig. 3 (D and E) illustrates an MT that grows throughout the sampling period and is simultaneously being translocated rearward at just under its rate of growth. This situation results in a net rate of MT advance of only ~1.6 μm min^{-1}, despite the fact that the MT is actually growing at >7 μm min^{-1}. This steady-state situation, in which persistent rearward MT translocation is superimposed on plus-end–directed MT growth, is very common. Note that near the

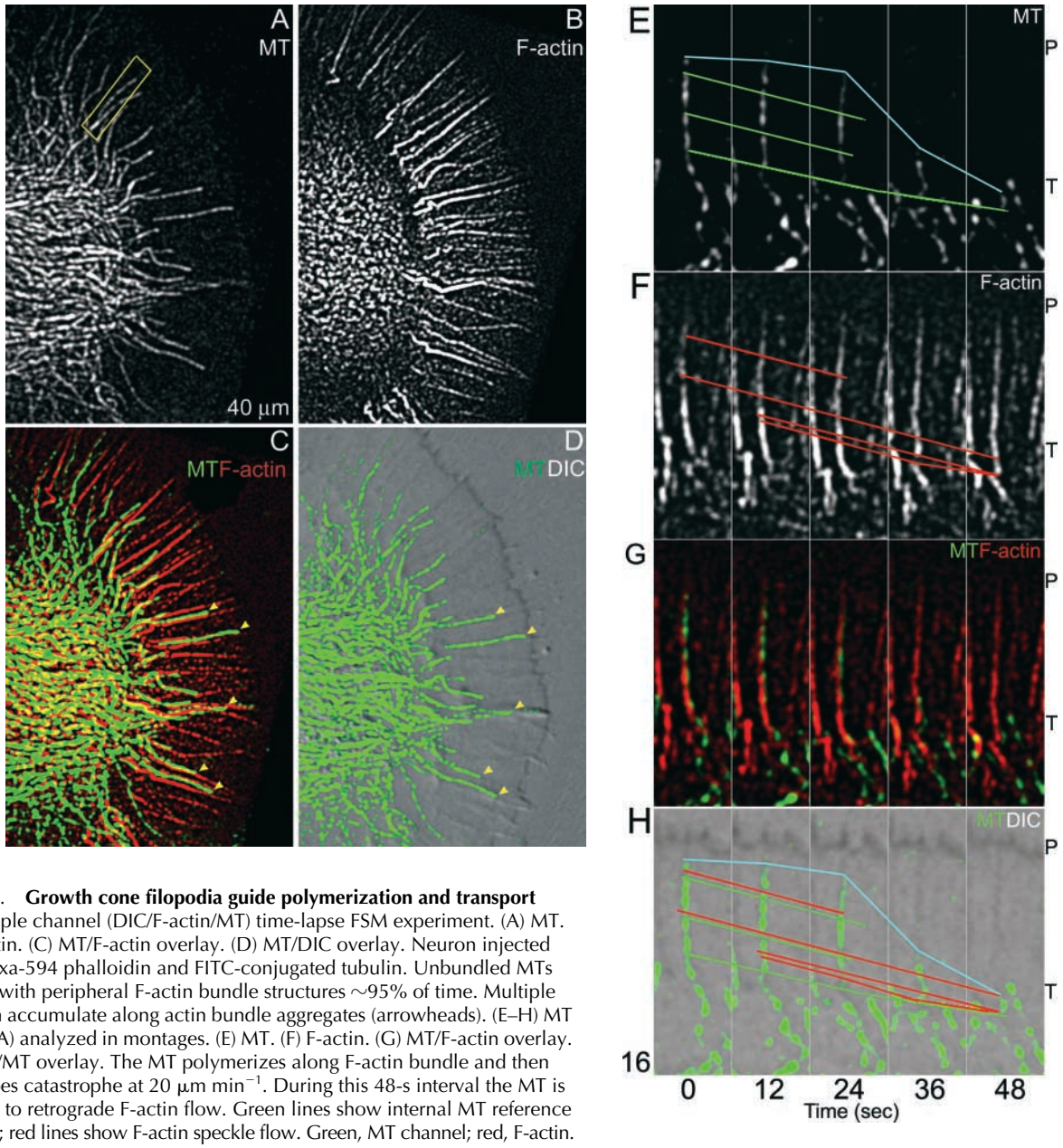

Figure 4. **Growth cone filopodia guide polymerization and transport MTs.** Triple channel (DIC/F-actin/MT) time-lapse FSM experiment. (A) MT. (B) F-actin. (C) MT/F-actin overlay. (D) MT/DIC overlay. Neuron injected with alexa-594 phalloidin and FITC-conjugated tubulin. Unbundled MTs aligned with peripheral F-actin bundle structures ~95% of time. Multiple MTs can accumulate along actin bundle aggregates (arrowheads). (E–H) MT in ROI (A) analyzed in montages. (E) MT. (F) F-actin. (G) MT/F-actin overlay. (H) DIC/MT overlay. The MT polymerizes along F-actin bundle and then undergoes catastrophe at 20 μm min^{-1}. During this 48-s interval the MT is coupled to retrograde F-actin flow. Green lines show internal MT reference speckles; red lines show F-actin speckle flow. Green, MT channel; red, F-actin.

90-s time point, a minus-end catastrophe occurs (Fig. 3, red line; D and E marks the minus end) and the MT rapidly shortens. In general, the dynamic parameters of MTs in the P-domain appeared similar to those described in other systems (Tanaka et al., 1995; Waterman-Storer and Salmon, 1997). In addition, we report the first observation of minus-end MT dynamics in neurons (Table I).

Filopodia are both MT polymerization guides and retrograde MT transporters

The striking correlation between retrograde MT translocation and retrograde F-actin flow rates prompted further investigation of MT–actin interactions. To this end, we used triple-channel multimode imaging that facilitated near simultaneous acquisition of MT and F-actin speckle data, and high-resolution differential interference contrast (DIC) images to record motility. Fig. 4 is an example of a DIC/F-actin/MT imaging experiment. Note that single MTs in the P-domain align predominantly along, or very near, filopodial F-actin bundles (Fig. 4 C, arrowheads; Video 7, available at http://www.jcb.org/cgi/content/full/jcb.200203038/DC1), and both cytoskeletal elements tend to align parallel to retrograde F-actin flow. MT alignment along filopodia is robust, occurring ~95% of time, although MTs can transiently detach from filopodia (Fig. 5). The DIC/MT overlays clearly show that MTs can penetrate deep into the P-domain, a fact often not appreciated in fixed preparations, as P-domain MTs are highly dynamic and not easily preserved (unpublished observations). MT–F-actin interactions in the ROI are shown in Fig. 4 (E–H; Video 8, available at http://www.jcb.org/cgi/content/full/jcb.200203038/DC1); an MT polymerizes along an F-actin bundle undergoing retrograde flow and then undergoes a catastrophe. Note that MT translocation is coupled to ret-

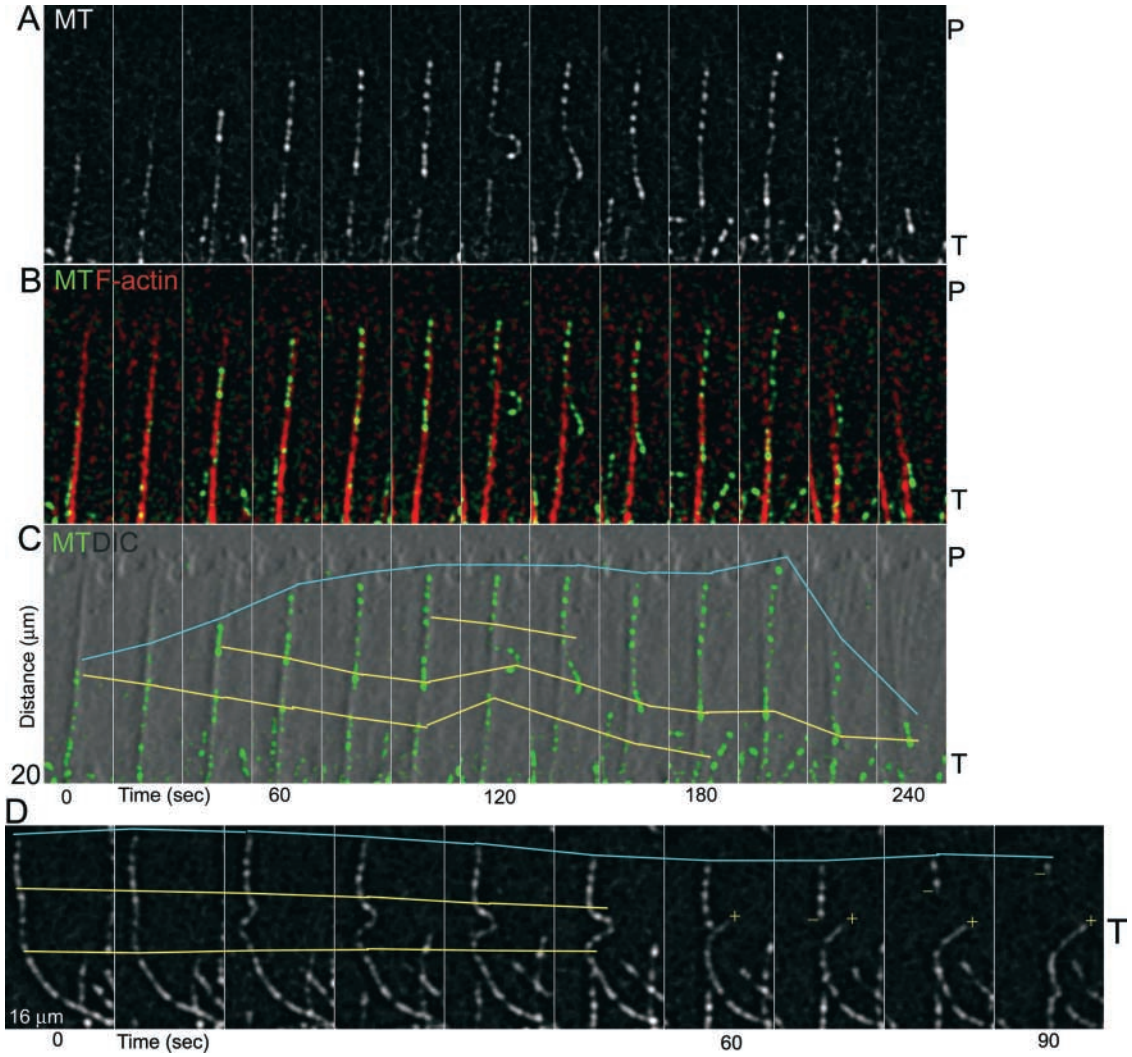

Figure 5. **MTs coupling to flow in P-domain leads to looping, breakage, and turnover.** (A–D) Time-lapse montages showing an example of a MT loop formation. (A) MT. (B) MT/F-actin overlay. (C) MT/DIC overlay. MT is aligned along prominent F-actin bundle and loop forms as proximal part of the MT translocates anterogradely (6.5 μm min^{-1}) and dissociates from actin bundle while the distal part of the MT is still aligned with cable (100–140 s). MT grows at a rate of 6.6 μm min^{-1} and then experiences a catastrophe and shortens at 14.6 μm min^{-1}. Green, MT channel; Red, F-actin. (D) MT loop formation and breakage sequence in the T-zone. Note minus-end catastrophe and plus-end growth immediately after break.

rograde F-actin flow most of the time (compare green and red line slopes). MTs can also transiently uncouple from retrograde flow. In Fig. 5 (A–C; Video 9, available at http://www.jcb.org/cgi/content/full/jcb.200203038/DC1), the MT is initially aligned along an actin bundle, and then at 120 s, the MT detaches and transiently forms a loop. This loop apparently results from a combination of an anterograde MT jump and persistent transport of the distal MT segment. The loop straightens out by 180 s as the MT reassociates with the F-actin bundle. Note that during loop formation, the MT plus end continues to grow and undergoes catastrophe >20 s after the loop had disappeared, suggesting distal plus-end MT behavior is independent of the more proximal looping activity. In some cases, loop formation is a prelude to MT breakage, as shown in Fig. 5 D (Video 10, available at http://www.jcb.org/cgi/content/full/jcb.200203038/DC1), where an MT is driven into the T-zone by retrograde flow where it buckles and then breaks. Note that the new plus end grows, whereas the minus end undergoes a catastrophe within 10 s after breakage. We also noted that MT breakage often occurred at the interface between the filopodia and actin arcs (Video 11, available at http://www.jcb.org/cgi/content/full/jcb.200203038/DC1).

In summary, under control conditions, MTs in the P-domain spend ~65% of time (49 MTs from 12 growth cones) tightly coupled to retrograde flow, and as a result, tend to be cleared from the P-domain as they grow. The rest of the time MTs either remain stationary and uncoupled from actin flow (15%) or exhibit localized translocation (20%; Fig. 8 B). These observations suggest that filopodial actin bundles act as MT polymerization guides that strongly bias MT growth trajectories and simultaneously mediate retrograde MT transport out of the P-domain. MT transport appears to cause compression, buckling, and MT breakage, in the T-zone. MT breakage generates new plus ends capable of growth, as well as distal fragments that tend to rapidly

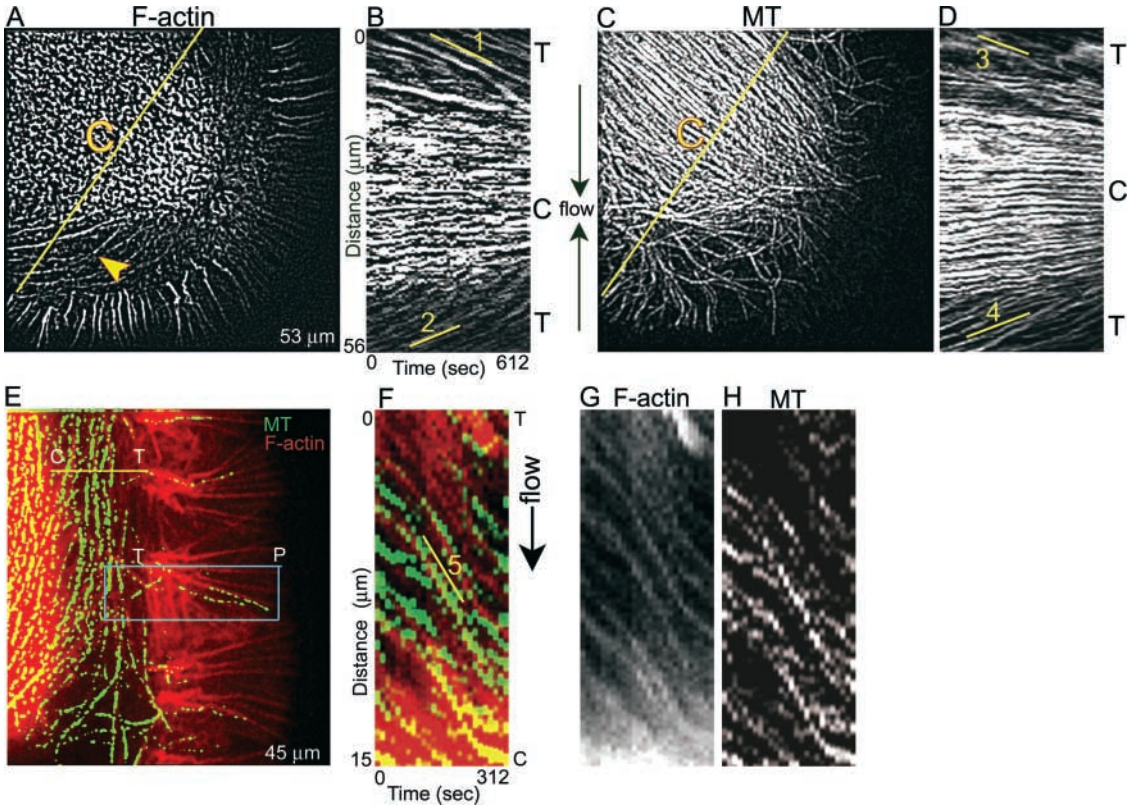

Figure 6. **MTs are packed into the C-domain via coupling to arc movements.** (A and C) Live growth cone showing prominent F-arcs (arrowhead) and MTs. C, C-domain. (B and D) Kymographs for F-actin and MT channels, respectively, generated from ROI marked by yellow lines. Both F-arcs and MTs translocate centripetally toward the central domain; actin line 1, 0.96 μm min^{-1}; line 2, 0.87 μm min^{-1}; MTs, line 3, 0.74 μm min^{-1}; line 4, 0.89 μm min^{-1}. (E) MT/F-actin overlay of another growth cone showing T zone filled with MTs and F-actin cables oriented transverse to MTs and F-actin bundles in P-domain. (F–H) Kymographs for MT–F-actin, F-actin, and MT, respectively, through ROI marked with yellow line in E. Retrograde flow rates of MTs and F-actin in T-zone are coupled. Line 5 slope, 1.7 μm min^{-1}.

turnover via minus-end catastrophes. We have not observed minus-end MT growth.

F-actin Arcs: a novel neuronal MT organizing structure

Live cell extraction–fixation protocols revealed a population of arc-like actin filament structures in the T-zone (Fig. 1). In FSM imaging studies, arcs, were most prominent on the lateral aspects of growth cones, where they undergo slow but persistent retrograde translocation. Fig. 6 A (Video 12, available at http://www.jcb.org/cgi/content/full/jcb.200203038/DC1) illustrates arc and MT (Fig. 6 C, arrowhead; Video 13, available at http://www.jcb.org/cgi/content/full/jcb.200203038/DC1) distributions in a live growth cone. To analyze arc movement, kymograph data was sampled in an ROI traversing lateral T-zones (yellow lines) for F-actin (Fig. 6 B) and MTs (Fig. 6 D). It is apparent that actin arcs and MTs both move towards the C-domain boundary, and that local rates and patterns of MT and arc movement are very similar, but not identical, indicating some rearrangement of MT–arc complexes can occur (compare slopes of lines 1 and 3 or 2 and 4). Fig. 6 E (Video 14, available at http://www.jcb.org/cgi/content/full/jcb.200203038/DC1) is an MT/F-actin overlay at higher magnification, illustrating coalignment of MTs and arcs in the T-zone. Kymographs sampled from the T-zone and into the C-domain (Fig. 6 E, yellow line), show arcs (Fig. 6, F and G) moving with the same trajectories as MTs (Fig. 6, F and H). Note that arcs and MTs decelerate in tandem as they enter the C-domain. These observations suggest that MTs are being transported into the C-domain via coupling to arc movements.

MTs associated with arcs are less dynamic than P-domain MTs

MTs that explore the P-domain tend to be highly dynamic, exhibiting rescue and catastrophe frequencies of 1.4 min^{-1} and 1 min^{-1}, respectively (Kabir et al., 2001). In contrast, we found MTs extending along the lateral borders of the axon and associated with arcs (Fig. 7 C, ROI) were much less dynamic. Indeed, they underwent catastrophes ~4 times less frequently, and rescues ~3.6 times more frequently than P-domain MTs; furthermore, their instantaneous rates of growth and shortening were much slower (Table I). This results in lateral MTs that grow slowly for extended periods; for example, the MT in Fig. 7 A (upper MT in ROI) alternates between growing and paused states, with no catastrophes for 7.5 min and extends ~20 μm.

Fig. 7 D (Video 15, available at http://www.jcb.org/cgi/content/full/jcb.200203038/DC1) is a time-lapse montage of the ROI (Fig. 7 C) and reveals an intriguing phenomenon. The sequence shows MTs polymerizing in opposite directions along the side of the distal axon shaft. One MT grows antero-

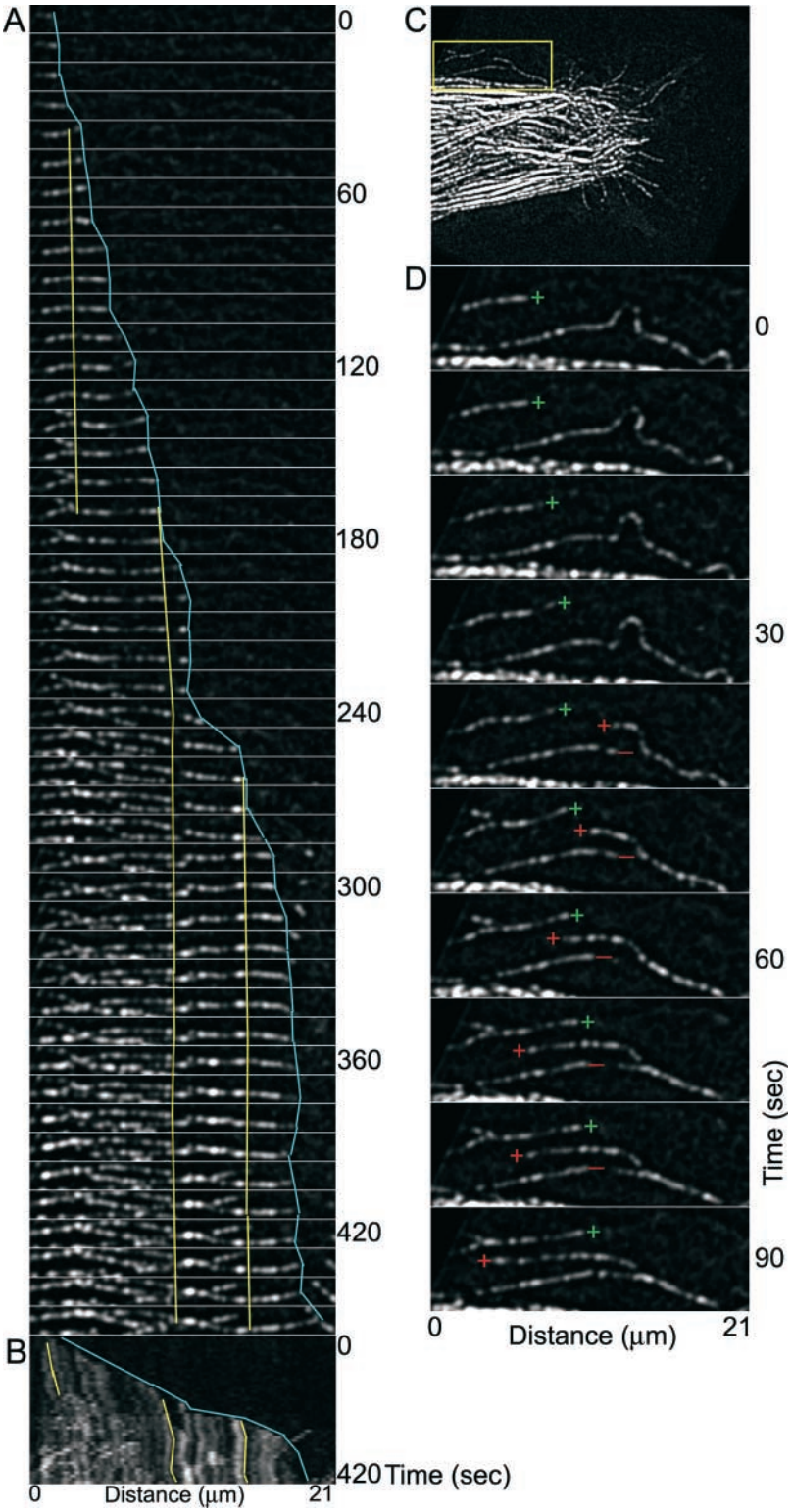

Figure 7. **Lateral arc associated MTs are much less dynamic than peripheral MTs and exhibit persistent growth.** The ROI is indicated in C and shown at higher magnification in D. (A) Time-lapse of the MT indicated with green + in D. This MT alternated between growth and pause, growing ~20 μm in 7.5 min with no catastrophes. Blue line follows distal speckle; yellow lines follow internal reference speckles. (B) Kymograph of A; note distance is on x axis to match panel above. (D) MTs forming antiparallel array polymerize in opposite directions. MT marked with green + grows toward the growth cone. Another MT breaks at 40 s and grows toward the cell body; new MT ends marked with red +/−.

gradely (marked with green +), and another initially intact MT kinks, breaks, and unexpectedly commences what appears to be plus-end growth towards the cell body. Given current interest in mechanisms for establishing neuronal process polarity (Baas, 2002) this behavior is worth mentioning. It appears that an antiparallel, i.e., dendrite-like, MT array is being generated from the distal end of the neurite by the novel mechanism of retrograde directed MT growth.

Discussion

We have characterized two specialized actin filament structures in growth cones, filopodia and actin arcs (Fig. 8 A, a and b), both of which interact strongly with MTs to regulate their behavior and distribution. We found that MTs exploring the P-domain exhibit the classic properties of dynamic instability (Mitchison and Kirschner, 1984) and use the polarized bundles of F-actin present in filopodia (Lewis and

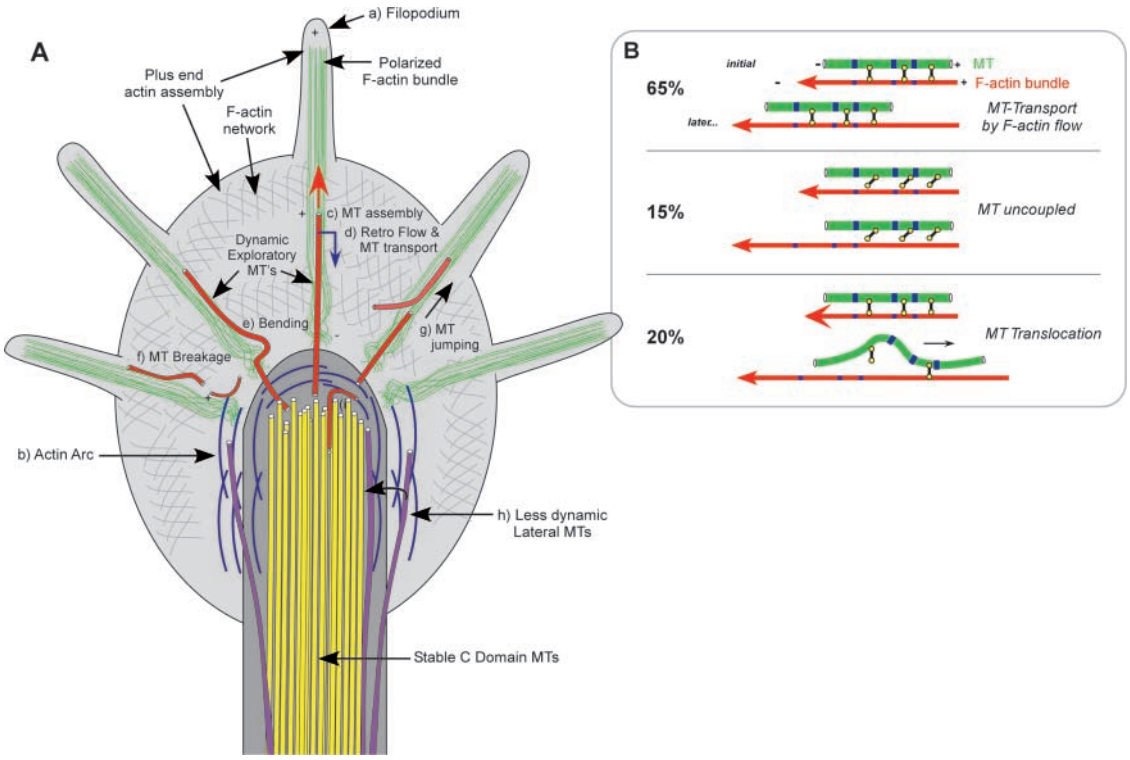

Figure 8. **Schematic emphasizing new structural and dynamics features of F-actin and MTs in the growth cone.** (A) The growth cone has two structurally and kinetically distinct zones of F-actin flow associated with filopodia in the P-domain and arcs in the T-zone. Both populations of F-actin serve as MT polymerization and translocation guides. Dynamic unbundled MTs polymerize into the periphery along filopodial F-actin bundles and are simultaneously cleared from the periphery by catastrophe and coupling to retrograde flow. A second much less dynamic population of MT is packed into the central domain axon shaft by coupling to transverse F-actin arc movements. (B) Types of MT-actin filament interactions with percentage of total time observed in each state.

Bridgman, 1992) as polymerization guides. The presence of F-actin bundles spanning the P-domain strongly biases the trajectories of MT advance, with an ~95% MT preference for filopodia versus intervening F-actin domains. From a functional standpoint, the radial distribution of filopodia promotes stochastic interrogation of the entire P-domain by MTs (e.g. Fig. 4, C and D [Video 7, available at http://www.jcb.org/cgi/content/full/jcb.200203038/DC1]). It is interesting to note that the population of MTs that invade the P-domain via filopodia are highly dynamic relative to T-zone MTs, suggesting functional specialization, perhaps in an exploratory and/or signaling capacity (see below; Kaverina et al., 1999).

In addition to their role in guiding MT advance, filopodia perform a second function, namely retrograde MT transport. Analysis of MT versus F-actin displacements revealed that MTs in the P-domain were transported rearward at essentially the same rate as surrounding F-actin ~65% of the time (Fig. 8 B). Filopodial F-actin and intervening networks both undergo myosin-dependent retrograde flow at the same rate in the P-domain (Fig. 2 A [Video 1, available at http://www.jcb.org/cgi/content/full/jcb.200203038/DC1]; Lin and Forscher, 1995; Lin et al., 1996), yet MTs strongly preferred filopodial actin bundles relative to intervening networks as transport substrates. These observations suggest that MTs are coupling to moving filopodial actin bundles via a specific interaction that mediates their transport. Of course, our data do not address whether this interaction is direct or indirect, although we would suspect the latter. Taken together, these results suggest that a second major function of filopodia is clearance of MTs from the P-domain. In addition, these results predict that the instantaneous position of an MT plus end in the P-domain will be determined by the rate of MT assembly minus the rate of retrograde F-actin flow (e.g., Fig. 8 A, c and d). Because MT dynamics and retrograde F-actin flow exist in a steady state, changes in the rate of either process will have predictable, rapid, and potentially robust effects given the rates of polymer flux involved. In support, we recently reported that PKC activation was correlated with an ~2.5-fold increase in MT growth lifetimes and that alteration of this MT assembly parameter alone resulted in a dramatic MT invasion of the P-domain (Kabir et al., 2001). It is also clear that MTs can transiently uncouple from retrograde flow (Fig. 5, A–C [Video 9, available at http://www.jcb.org/cgi/content/full/jcb.200203038/DC1]) and remain stationary (15% of the time; Fig. 8 B) or exhibit localized jumping (20% of the time; Fig. 8 A, g). MTs can also jump from one filopodium track to another (Video 11, available at http://www.jcb.org/cgi/content/full/jcb.200203038/DC1). Characterization of the molecular substrates that mediate MT–actin filament coupling and the molecular motors implicated by MT jumping events will be of keen interest. Given recent reports, an interesting possibility for maintaining and/or directing MTs down the polarized filopodial bundles, would be an MT end binding complex containing myosin and kinesin functionality (Yin et al., 2000; Karcher et al., 2002).

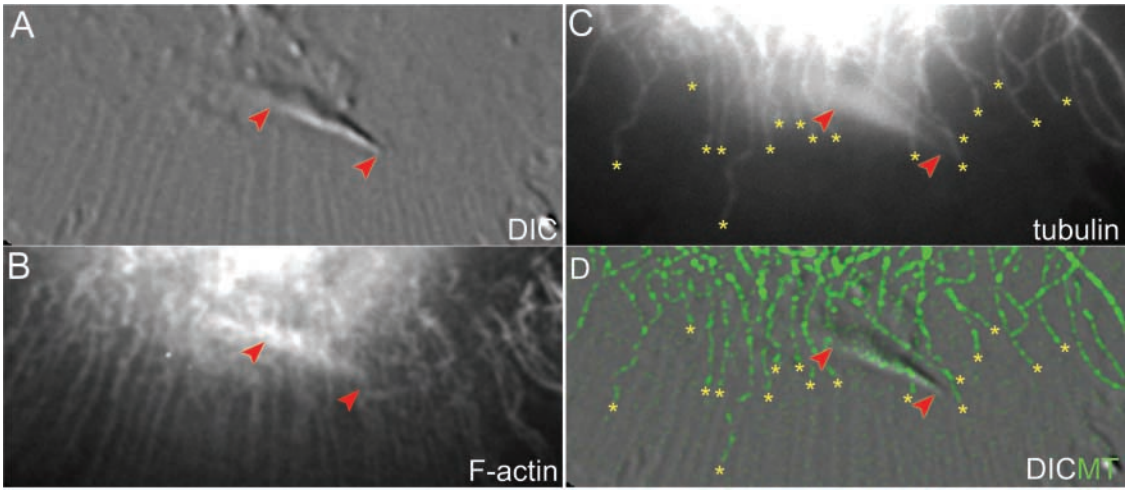

Figure 9. **MTs enter the P-domain independently of intrapodia.** (A) DIC and (B) F-actin images from a live growth cone showing an intrapodia marked with red arrows moving from left to right and out of T-zone. (C) Image of the unprocessed tubulin channel showing significant levels of diffuse tubulin signal associated with the intrapodia due to increased volume in the area. (D) DIC and processed tubulin channel overlay of the same area. Yellow asterisks mark MT ends in C and D. Note the volume artifact present after image processing to enhance MT structures; the tapered structure between the red arrowheads in D is distinct from MTs that have uniform caliber, and results from diffusible tubulin label in the volume of a protruding F-actin structure (Videos 16 and 17, available at http://www.jcb.org/cgi/content/full/jcb.200203038/DC1).

A second major function of retrograde flow appears to be MT turnover. MTs form loops, which can buckle and break as they are transported rearward into the T-zone (Figs. 8 A, d–f). Our results strongly suggest that retrograde flow exerts compressive forces on MTs. This often occurs when MTs coupled to retrograde F-actin flow enter the T-zone where the flow rate slows abruptly and the distal MT segment is being moved at a faster rate that the proximal segment; under these circumstances, a kink that can lead to breakage is likely to form (Fig. 5 D [Video 10, available at http://www.jcb.org/cgi/content/full/jcb.200203038/DC1]; Video 11, available at http://www.jcb.org/cgi/content/full/jcb.200203038/DC1). MT breakage also results in exposure of new plus ends which tend to regrow, and minus ends which rapidly undergo catastrophes. The net result is efficient MT turnover in the P-domain. Because virtually nothing is known about the mechanism of MT turnover in growth cones, and minus-end dynamics have never been reported before, these results provide the first step in the characterization of these processes. Interestingly, similar observations have been made in the convergence zone of migrating epithelial cells (Salmon et al., 2002), suggesting conservation of a fundamental mechanism for MT turnover and plus-end generation in diverse cell types.

We also describe a novel role for F-actin arcs in MT organization and transport. Arcs were detected in the T-zone in both fixed and living growth cones and exhibited persistent retrograde movement into the C-domain at rates similar to those previously reported in fibroblasts (Heath, 1983) which are ~1/4 the rate of P-domain retrograde flow. We found arcs interact strongly with a population of MTs roughly perpendicular to those extending along filopodial actin bundles (Fig. 8 A, h). Arcs form a hemicircumferential ring network within the T-zone (Fig. 8 A, b) and are most easily observed on the sides of growth cones (e.g., Figs. 1 a and 6 a, arrowheads). This is in part due to the presence of intense ruffling/intrapodia activity often observed in the T-zone sector aligned with the axis of growth cone advance (Fig. 1 A, red star). Ruffling involves barbed-end–directed actin assembly (Forscher et al., 1992; Rochlin et al., 1999), which tends to mask the presence of arcs. Interestingly, lateral arc-associated MTs have slower instantaneous growth rates than P-domain MTs; however, they grow quite efficiently by virtue of dramatically reduced catastrophe and increased rescue frequencies. The mechanism(s) underlying these differences remains to be determined; however, we speculate that because P-domain MTs provide rapid stochastic sampling of P-domain space they may serve in a signal transduction capacity (Kirschner and Mitchison, 1986), whereas arc-associated MTs may provide stable, sustained growth to promote axon elongation. Note that as the axon grows, arc-associated MTs are also steadily being delivered and packed into the lateral aspect of the C-domain (Figs. 6 and 8 h), perhaps as a prelude to crosslinking by MT-associated proteins and their maturation into stable MTs.

It was recently reported that actin filaments and MTs undergo coordinated assembly and disassembly in cultured cortical neuron growth cones (Dent and Kalil, 2001). Specifically, extension and shrinkage of F-actin ruffles/intrapodia from the T-zone were correlated with processes proposed to be MTs. In contrast, we found no correlation between F-actin disassembly and MT catastrophes; in fact, most plus-end catastrophes occurred in the P-domain, when MT ends were closely associated with stable filopodial F-actin structures undergoing retrograde flow (e.g., Fig. 4, E–H [Video 8, available at http://www.jcb.org/cgi/content/full/jcb.200203038/DC1]) and nowhere near shrinking actin ruffles. We also looked carefully for coordinated MT and actin assembly. Because of ruffling activity, the T-zone has significant z axis height, and thus presents two challenges for assessing polymer dynamics: (1) time-dependent volume artifacts are present when using diffusible probes; and (2) cytoskeletal elements can move in and out of the optical z section, generating movement artifacts. Volume artifacts are

minimized when the probe has higher affinity for polymer than monomer, as is the case with phalloidin. However, for tubulin, significant concentrations of bound and free labeled subunits coexist. This can be appreciated in Fig. 9 (Videos 16 and 17, available at http://www.jcb.org/cgi/content/full/jcb.200203038/DC1), in which a protruding F-actin ruffle is shown (A and B, arrowheads). Fig. 9 C shows the unprocessed tubulin channel; note the significant level of diffuse tubulin signal within the ruffle volume (arrowheads). Note also the many linear elements present (Fig. 9 C, asterisks) which are revealed as bona fide specked MTs after image processing (Fig. 9 D); in addition, a volume artifact is present after image processing. Specifically, the tapered structure between the arrowheads in Fig. 9 D is undoubtedly labeled tubulin dimer occupying the diffusible volume of the protruding F-actin ruffle (e.g., Video 16, available at http://www.jcb.org/cgi/content/full/jcb.200203038/DC1). Such structures are similar to those reported to be MTs (Dent and Kalil, 2001) and would indeed appear to copolymerize and codepolymerize with F-actin. We excluded such structures in our analysis and perusal of a large population of MT assembly events (e.g., Video 17, available at http://www.jcb.org/cgi/content/full/jcb.200203038/DC1), suggests that formation MT–actin complexes by copolymerization is an unlikely event in our system. Our results do not rule out a role for MT ends in regulating focal actin assembly and are consistent with those of Rochlin et al. (1999), who reported MT ends near sites of intrapodia initiation (but not along their length), but also found that MT polymerization was neither necessary nor sufficient for intrapodia formation (Rochlin et al., 1999). Note that the intrapodium propagating from left to right in Fig. 9 (A and B) has weak phalloidin labeling near the site of actin assembly (right arrowhead) and increased labeling in its tail (left arrowhead) containing older filaments–consistent with relatively slow filament labeling by alexa-phalloidin. This was not problematic in the current study which focused on analysis of retrograde flow rates, but could pose problems for assessing events with short actin filament lifetimes.

A central theme emerging from the current study is that actin filament structures organize the distribution and behavior of MTs in the growth cone. Interestingly, recent evidence suggests that processes as diverse as wound healing and cell migration employ strikingly similar MT organizing strategies (Craig Mandato and William Bement, personal communication; Salmon et al., 2002). In all three systems, self-assembling actomyosin networks generate F-actin flow patterns that mediate MT transport and appear to play a role in regulating MT turnover and dynamics. Functional differences, where they exist, may arise from specialized actin filament geometries rather than fundamental mechanistic differences. For example, in growth cones, it appears that the P-domain may be functionally equivalent to the lamellipodium of a typical motile cell, with an added specialization (filopodia) for radial distribution of MT trajectories. Given that filopodia appear to be related to microspikes (Small et al., 2002), it will be interesting to see if cells with prominent microspikes impose similar guidance effects on MTs.

What is the functional significance of the intimate MT–actin interactions observed in filopodia? Dynamic instability provides an efficient mechanism for MTs to stochastically sample the P domain. An intriguing possibility is that exploratory MTs tracking down filopodia could be selectively stabilized (or destabilized) in response to local signals (Kirschner and Mitchison, 1986). Alternatively, MTs might deliver signals to modulate cell adhesion or membrane-cytoskeletal interactions (Kaverina et al., 1999). In this context, it is interesting to note that filopodia can indeed initiate interactions that result in MT advance toward growth cone target sites in vitro and in vivo (Lin and Forscher, 1993; O'Connor and Bentley, 1993). Additionally, we have shown that retrograde F-actin flow slows (Lin and Forscher, 1995) as traction force develops between a target substrate and the growth cone's internal contractile machinery (Suter et al., 1998). The current findings suggest that during such interactions, MTs will advance efficiently and specifically down filopodia in response to even a slight decrease in retrograde flow.

Materials and methods

Cell culture and chemicals

Primary culture of *Aplysia* bag cell neurons was as previously described (Forscher et al., 1987) with the following modifications. For multimode microscopy, phenol containing L15 medium (Life Technologies) with artificial seawater (ASW) was replaced with phenol-free L15-ASW supplemented with 1 mg/ml BSA, 1 mg/ml L-carnosine, 500 nM vitamin E, and 500 μM n-t-butyl-α-phenyl-nitrone (BPN) to decease photobleaching and photodamage. All chemical were purchased from Sigma-Aldrich or Calbiochem.

Immunocytochemistry

Cultured bag cell neurons were extracted live and chemically fixed as follows: cells were washed with Ca^{2+}-free low–ionic strength ASW (100 mM NaCl, 10 mM KCl, 5 mM $MgCl_2$, 15 mM Hepes, 60 g/L glycine, pH 7.9) containing 5 mM EGTA for 2 min then extracted with 1% Triton X-100 in cytoskeletal stabilization buffer containing: 80 mM Pipes, 5 mM EGTA, 1 mM $MgCl_2$, 10 uM Taxol, 1 uM Alexa 594-phalloidin (Molecular Probes) plus 4% PEG (MW 35,000) for 1 min. After washing with CSB, cells were fixed with 3.7% formaldehyde in CSB. Both groups were double labeled for F-actin and MTs. For MTs, an mAb TUB.21 (Sigma-Aldrich) and Alexa-488 goat anti–mouse secondary was used. Double-labeled samples were imaged on a Nikon Eclipse TE300 microscope with a Coolsnap HQ cooled CCD camera (Roper Scientific) using MetaMorph control software (Universal Imaging).

EM

After extracting live cells, bag cell neurons were fixed sequentially with 2% glutaraldehyde plus 10 mM lysine, 0.5% osmium tetroxide, 0.2% uranyl acetate, and 0.3% lead citrate. Cells were then dehydrated with graded ethanol and critical point dried. Rotary shadowing was performed with tungsten using electron-bombardment technology. Replicas were mounted on formvar-coated EM grids after separating them with hydrofluoric acid and observed with a transmission EM at 60 kV. Immunoelectron microscopy was performed similar to immunocytochemical methods except for incubation with secondary antibodies, in which case 15-nm gold-labeled anti–mouse IgG was performed for 15 h at room temperature.

F-actin and MT dynamics and multimode microscopy

F-actin and MT dynamics were assessed using FSM (Waterman-Storer and Salmon, 1998; Waterman-Storer et al., 1998). We previously demonstrated retrograde F-actin flow can be assessed by fluorescence photobleaching using either fluorescently labeled G-actin or phalloidin with essentially equivalent results, provided the latter probe was injected at sufficiently low concentrations (Lin and Forscher, 1995). Thus, for assessing F-actin dynamics, neurons were injected with 20 μM Alexa-488 or Alexa-594 phalloidin. Typically, <10% of cell volume was injected, yielding final cell concentrations of phalloidin ~2 μM. The 6.6-μM Alexa-phalloidin methanol stock was dried, redissolved, and diluted in injection buffer to the appropriate concentration prior to use. Similar results were obtained using rhodamine-conjugated G-actin (Lin and Forscher, 1995). For MT dynamics, neurons

were injected with ~1 mg/ml rhodamine or FITC-labeled tubulin (Cytoskeleton, Inc.) in injection buffer (100 mM Pipes; 1 mM $MgCl_2$; 1 mM EGTA) and allowed to recover ~60 min in L15-ASW medium. Under these conditions, MT speckles could be clearly discerned in distal axonal regions and used as fiducial marks. Care was taken to only analyze single unbundled MTs where distinct linear arrays of speckles could be followed over time. Estimated thickness of the periperhal lamella (~300 nm) is close to the optical resolution of ~230 nm for the rhodamine-labeled MTs; however, in the T-zone and C-domain, cell thickness can increase to >1 μm. In these domains, the appearance and disappearance of speckles could result from changes in the Z axis of the MT, so measurements were limited to thin regions on the sides of the growth cone. MT image sequences were obtained using a Nikon Eclipse TE300 microscope equipped with a Photometrics Quantix 57 back illuminated frame transfer cooled CCD camera mounted on the bottom port. Two programmable fast filter wheels (100-ms filter changes) that include shutters were mounted with bandpass filters (Ludl, Inc.) for changing both excitation and emission wavelengths. The DIC analyzer was moved to the emission filter wheel for switching between fluorescence to DIC imaging modes. A harmonic mirror with reflective bands corresponding to FITC or rhodamine excitation maxima replaced the normal epifluorescence dichroic mirror. Metamorph control software (Universal Imaging) was used for instrument control and image analysis. Images were recorded every 5–20 s using ~500-ms integration times for fluorescent MTs and F-actin and 50 ms for DIC. Contrast of the MT speckles was enhanced by processing the fluorescent images with the following spatial filters: unsharp mask, low pass, laplace edge enhancement, and a final low pass. For F-actin speckles, unsharp mask and low pass spatial filters were used to enhance contrast. For DIC-fluorescent overlays, a threshold look up table was applied to MT images before combining with the DIC image to clear low level background noise. Stacks of time-lapse images were converted into movies, time-lapse montages, and kymographs for data analysis. The Metamorph kymograph function creates a time versus space plot of intensity values for a user-defined line scan of variable width. In order to detect displacement, the line scan must be oriented along the axis of movement. Line scans were standardized at a width of 10 pixels (~1 μm actual size on the CCD faceplate) and the average grayscale value within that the sampling region was plotted as a function of time. Distances and x,y coordinates were exported to MS Excel for analysis.

Online supplemental material

All videos are available online at http://www.jcb.org/cgi/content/full/jcb.200203038/DC1.

We extend our appreciation to Drs. Clare Waterman-Storer, Bill Bement, and members of their laboratories for sharing unpublished results, scientific insights, and lively dinner conversation. We also thank Drs. Tom Pollard, Tim Mitchison, and John Heuser for critical comments and encouragement in pursuing ultrastructural studies.

This work supported by National Institutes of Health grant RO1-NS28695 to P. Forscher, and postdoctoral fellowship NS1F32 NS11122 to A.W. Schaefer.

Submitted: 8 March 2002
Revised: 13 May 2002
Accepted: 30 May 2002

References

Baas, P.W. 2002. Microtubule transport in the axon. *Int. Rev. Cytol.* 212:41–62.

Bentley, D., and A. Toroian-Raymond. 1986. Disoriented pathfinding by pioneer neurone growth cones deprived of filopodia by cytochalasin treatment. *Nature.* 323:712–715.

Bray, D. 1979. Mechanical tension produced by nerve cells in tissue culture. *J. Cell Sci.* 37:391–410.

Bush, M.S., R.G. Goold, F. Moya, and P.R. Gordon-Weeks. 1996. An analysis of an axonal gradient of phosphorylated MAP 1B in cultured rat sensory neurons. *Eur. J. Neurosci.* 8:235–248.

Challacombe, J.F., D.M. Snow, and P.C. Letourneau. 1996. Actin filament bundles are required for microtubule reorientation during growth cone turning to avoid an inhibitory guidance cue. *J. Cell Sci.* 109:2031–2040.

Challacombe, J.F., D.M. Snow, and P.C. Letourneau. 1997. Dynamic microtubule ends are required for growth cone turning to avoid an inhibitory guidance cue. *J. Neurosci.* 17:3085–3095.

Davenport, R.W., P. Dou, V. Rehder, and S.B. Kater. 1993. A sensory role for neuronal growth cone filopodia. *Nature.* 361:721–724.

De La Cruz, E.M., and T.D. Pollard. 1996. Kinetics and thermodynamics of phalloidin binding to actin filaments from three divergent species. *Biochemistry.* 35:14054–14061.

Dent, E.W., and K. Kalil. 2001. Axon branching requires interactions between dynamic microtubules and actin filaments. *J. Neurosci.* 21:9757–9769.

Forscher, P., and S.J. Smith. 1988. Actions of cytochalasins on the organization of actin filaments and microtubules in a neuronal growth cone. *J. Cell Biol.* 107:1505–1516.

Forscher, P., and S.J. Smith. 1990. Cytoplasmic actin filaments move particles on the surface of a neuronal growth cone. *In* Optical Microscopy for Biology. B. Herman and K. Jacobson, editors. Wiley Liss, Inc., New York. 990:459–471.

Forscher, P., L.K. Kaczmarek, J.A. Buchanan, and S.J. Smith. 1987. Cyclic AMP induces changes in distribution and transport of organelles within growth cones of Aplysia bag cell neurons. *J. Neurosci.* 7:3600–3611.

Forscher, P., C.H. Lin, and C. Thompson. 1992. Novel form of growth cone motility involving site-directed actin filament assembly. *Nature.* 357:515–518.

Gomez, T.M., E. Robles, M. Poo, and N.C. Spitzer. 2001. Filopodial calcium transients promote substrate-dependent growth cone turning. *Science.* 291: 1983–1987.

Gordon-Weeks, P.R. 1991. Evidence for microtubule capture by filopodial actin filaments in growth cones. *Neuroreport.* 2:573–576.

Heath, J.P. 1983. Behaviour and structure of the leading lamella in moving fibroblasts. I. Occurrence and centripetal movement of arc-shaped microfilament bundles beneath the dorsal cell surface. *J. Cell Sci.* 60:331–354.

Kabir, N., A.W. Schaefer, A. Nakhost, W.S. Sossin, and P. Forscher. 2001. Protein kinase C activation promotes microtubule advance in neuronal growth cones by increasing average microtubule growth lifetimes. *J. Cell Biol.* 152:1033–1044.

Karcher, R.L., S.W. Deacon, and V.I. Gelfand. 2002. Motor-cargo interactions: the key to transport specificity. *Trends Cell Biol.* 12:21–27.

Kaverina, I., O. Krylyshkina, and J.V. Small. 1999. Microtubule targeting of substrate contacts promotes their relaxation and dissociation. *J. Cell Biol.* 146: 1033–1044.

Kirschner, M., and T. Mitchison. 1986. Beyond self-assembly: from microtubules to morphogenesis. *Cell.* 45:329–342.

Lamoureux, P., R.E. Buxbaum, and S.R. Heidemann. 1989. Direct evidence that growth cones pull. *Nature.* 340:159–162.

Letourneau, P.C. 1983. Differences in the organization of actin in the growth cones compared with the neurites of cultured neurons from chick embryos. *J. Cell Biol.* 97:963–973.

Lewis, A.K., and P.C. Bridgman. 1992. Nerve growth cone lamellipodia contain two populations of actin filaments that differ in organization and polarity. *J. Cell Biol.* 119:1219–1243.

Lin, C.H., and P. Forscher. 1993. Cytoskeletal remodeling during growth cone-target interactions. *J. Cell Biol.* 121:1369–1383.

Lin, C.H., and P. Forscher. 1995. Growth cone advance is inversely proportional to retrograde F-actin flow. *Neuron.* 14:763–771.

Lin, C.H., C.A. Thompson, and P. Forscher. 1994. Cytoskeletal reorganization underlying growth cone motility. *Curr. Opin. Neurobiol.* 4:640–647.

Lin, C.H., E.M. Espreafico, M.S. Mooseker, and P. Forscher. 1996. Myosin drives retrograde F-actin flow in neuronal growth cones. *Neuron.* 16:769–782.

Marsh, L., and P.C. Letourneau. 1984. Growth of neurites without filopodial or lamellipodial activity in the presence of cytochalasin B. *J. Cell Biol.* 99:2041–2047.

Mitchison, T., and M. Kirschner. 1984. Dynamic instability of microtubule growth. *Nature.* 312:237–242.

O'Connor, T.P., and D. Bentley. 1993. Accumulation of actin in subsets of pioneer growth cone filopodia in response to neural and epithelial guidance cues in situ. *J. Cell Biol.* 123:935–948.

Rochlin, M.W., K.M. Wickline, and P.C. Bridgman. 1996. Microtubule stability decreases axon elongation but not axoplasm production. *J. Neurosci.* 16: 3236–3246.

Rochlin, M.W., M.E. Dailey, and P.C. Bridgman. 1999. Polymerizing microtubules activate site-directed F-actin assembly in nerve growth cones. *Mol. Biol. Cell.* 10:2309–2327.

Sabry, J.H., T.P. O'Connor, L. Evans, A. Toroian-Raymond, M. Kirschner, and D. Bentley. 1991. Microtubule behavior during guidance of pioneer neuron growth cones in situ. *J. Cell Biol.* 115:381–395.

Salmon, W.C., M.C. Adams, and C.M. Waterman-Storer. 2002. Dual-wavelength fluorescent speckle microscopy reveals coupling of microtubule and actin movements in migrating cells. *J. Cell Biol.* 158:31–37.

Small, J.V., T. Stradal, E. Vignal, and K. Rottner. 2002. The lamellipodium: where motility begins. *Trends Cell Biol.* 12:112–120.

Song, H.J., and M.M. Poo. 1999. Signal transduction underlying growth cone guidance by diffusible factors. *Curr. Opin. Neurobiol.* 9:355–363.

Suter, D.M., L.D. Errante, V. Belotserkovsky, and P. Forscher. 1998. The Ig superfamily cell adhesion molecule, apCAM, mediates growth cone steering by substrate-cytoskeletal coupling. *J. Cell Biol.* 141:227–240.

Suter, D.M., and P. Forscher. 2000. Substrate-cytoskeletal coupling as a mechanism for the regulation of growth cone motility and guidance. *J. Neurobiol.* 44:97–113.

Svitkina, T.M., A.B. Verkhovsky, and G.G. Borisy. 1995. Improved procedures for electron microscopic visualization of the cytoskeleton of cultured cells. *J. Struct. Biol.* 115:290–303.

Tanaka, E., and M.W. Kirschner. 1995. The role of microtubules in growth cone turning at substrate boundaries. *J. Cell Biol.* 128:127–137.

Tanaka, E., T. Ho, and M.W. Kirschner. 1995. The role of microtubule dynamics in growth cone motility and axonal growth. *J. Cell Biol.* 128:139–155.

Waterman-Storer, C.M., and E.D. Salmon. 1997. Actomyosin-based retrograde flow of microtubules in the lamella of migrating epithelial cells influences microtubule dynamic instability and turnover and is associated with microtubule breakage and treadmilling. *J. Cell Biol.* 139:417–434.

Waterman-Storer, C.M., and E.D. Salmon. 1998. How microtubules get fluorescent speckles. *Biophys. J.* 75:2059–2069.

Waterman-Storer, C.M., A. Desai, J.C. Bulinski, and E.D. Salmon. 1998. Fluorescent speckle microscopy, a method to visualize the dynamics of protein assemblies in living cells. *Curr. Biol.* 8:1227–1230.

Williamson, T., P.R. Gordon-Weeks, M. Schachner, and J. Taylor. 1996. Microtubule reorganization is obligatory for growth cone turning. *Proc. Natl. Acad. Sci. USA.* 93:15221–15226.

Yin, H., D. Pruyne, T.C. Huffaker, and A. Bretscher. 2000. Myosin V orientates the mitotic spindle in yeast. *Nature.* 406:1013–1015.